

# From Text to Forecasts: Bridging Modality Gap with Temporal Evolution Semantic Space

Lehui Li<sup>1,\*</sup>, Yuyao Wang<sup>2,\*</sup>, Jisheng Yan<sup>1</sup>, Wei Zhang<sup>1</sup>, Jinliang Deng<sup>3,4,†</sup>, Haoliang Sun<sup>1</sup>, Zhongyi Han<sup>1</sup>, Yongshun Gong<sup>1,†</sup>

<sup>1</sup>School of Software, Shandong University, China

<sup>2</sup>Boston University, Boston, MA, USA

<sup>3</sup>State Key Laboratory of Complex & Critical Software Environment, Beihang University

<sup>4</sup>Research Institute of Trustworthy Autonomous Systems, SUSTech

Correspondence to: jinliangdeng9588@gmail.com, ysgong@sdu.edu.cn

\*Equal contribution. †Co-corresponding authors.

**Abstract.** Incorporating textual information into time-series forecasting holds promise for addressing event-driven non-stationarity; however, a fundamental modality gap hinders effective fusion: textual descriptions express temporal impacts implicitly and qualitatively, whereas forecasting models rely on explicit and quantitative signals. Through controlled semi-synthetic experiments, we show that existing methods over-attend to redundant tokens and struggle to reliably translate textual semantics into usable numerical cues. To bridge this gap, we propose TESS, which introduces a Temporal Evolution Semantic Space as an intermediate bottleneck between modalities. This space consists of interpretable, numerically grounded temporal primitives—mean shift, volatility, shape, and lag—extracted from text by an LLM via structured prompting and filtered through confidence-aware gating. Experiments on four real-world datasets demonstrate up to a 29% reduction in forecasting error compared to state-of-the-art uni-modal and multimodal baselines. The code will be released after acceptance.

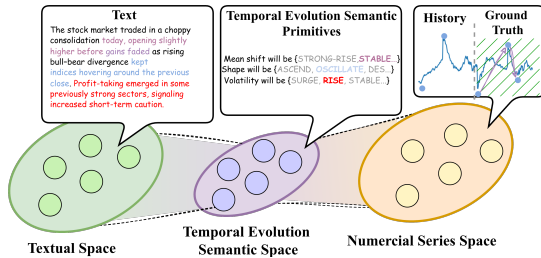


Figure 1: Illustration of the cross-modal transformation via the Temporal Semantic Space. Verbose textual narratives (left) are distilled into structured temporal primitives (middle), which then guide numerical forecasting (right).

## 1 Introduction

Time-series forecasting plays a critical role in diverse domains such as transportation, energy, and finance [Zhou et al., 2021, Wang et al., 2025a]. In recent years, unimodal forecasting models that rely solely on historical numerical observations have achieved substantial progress by modeling temporal dependencies [Wu et al., 2021]. However, real-world time series often exhibit significant non-stationarity [Du et al., 2021, Kim et al., 2025], where the underlying data-generating mechanism evolves over time. In

particular, exogenous events such as accidents, extreme weather, or public sentiment shocks can trigger regime shifts [Osogami, 2021, Yang et al., 2025], causing statistical properties—including trends, volatility, mean, and variance—to change abruptly within short time windows [An et al., 2025]. Under such conditions, models struggle to extract reliable predictive signals from historical numerical observations alone, leading to severe performance degradation [Zeng et al., 2023].

To mitigate event-driven non-stationarity, recent work has begun to incorporate textual data (e.g. news articles, social media posts) [Sawhney et al., 2020], as an exogenous information source. The typical approach leverages pretrained language models to encode text into semantic embeddings [Niu et al., 2023], which are then fused with numerical time-series features via concatenation, gating, or cross-modal attention [Sawhney et al., 2020, Koval et al., 2025]. These multimodal methods have demonstrated notable gains on benchmarks with significant non-stationarity.

Despite recent progress, the substantial *modality gap* [Liang et al., 2022] between time series data and textual data remains largely overlooked [Koval et al., 2025], fundamentally limiting multimodal forecasting. Time series data is chronologically ordered and quan-

titative, offering precise measurements of temporal dynamics, yet it lacks explicit semantic abstraction. In contrast, textual data is semantically rich but unstructured and qualitative, with the impacts of events on temporal dynamics often implicit, diffuse, and weakly grounded in time. As a result, the predictive relevance of textual information is sparsely distributed across tokens and rarely aligned with the compact numerical structure required by time-series models. Through controlled semi-synthetic experiments, we analyze time-series predictors that directly fuse numerical observations with raw textual embeddings. We find that: (1) predictors fail to focus on prediction-relevant tokens, instead being distracted by noisy and redundant textual content; (2) even after removing redundant information, models still struggle to correctly decode temporal evolution signals, indicating a fundamental representational mismatch between the two modalities.

To bridge this modality gap, As illustrated in Figure 1, we propose to construct an intermediate representation between the textual space and the numerical series space, termed the *Temporal Evolution Semantic Space*. This space serves as an information bottleneck that explicitly filters, structures, and organizes textual information relevant to temporal evolution. Inspired by expert-driven paradigms in temporal pattern analysis, we predefine a set of temporal evolution primitives corresponding to critical attributes governing temporal dynamics, such as mean shift, volatility shift, evolution shape, and lag. Crucially, these primitives are expressed as verbal specifications, enabling large language models (LLMs) to emulate human-like judgments when interpreting textual descriptions of events. We decompose the fusion process into two stages: ① **Text**  $\rightarrow$  **Semantic Space**: We prompt an LLM to reason over the input text and explicitly label latent temporal evolution signals using the predefined primitives. Since such labels may be unreliable due to information insufficiency or limitations of the LLM, we introduce a learnable gating network to estimate and weight the reliability of the generated semantic labels. ② **Semantic Space**  $\rightarrow$  **Numerical Space**: The inferred temporal evolution primitives are then injected as exogenous conditions into the time-series model, allowing it to leverage its numerical modeling and pattern recognition capabilities to ground semantic signals in observed temporal dynamics. Our **contributions** are summarized as follows:

- Through semi-synthetic experiments, we identify two bottlenecks in text-time-series fusion: attention is distracted by redundant context, and qualitative expressions resist decoding into predictive

gains.

- We propose TESS, an intermediate space that distills text into temporal primitives via LLM extraction with confidence-aware gating, guiding forecasters as exogenous conditions.
- Experiments on four datasets show up to 29% MSE reduction; analyses validate primitive complementarity and gating effectiveness across non-stationary patterns.

## 2 Related Work

**Uni-Modal Time-Series Forecasting.** Early time series forecasting relies on classical statistical methods that extrapolate trends under stationarity assumptions Chen et al. [2004], Huang and Shih [2003], Kalekar et al. [2004], performing well on smaller, simpler datasets. Deep learning models Wang et al. [2025a], Deng et al. [2024], Zhou et al. [2022] have since enabled end-to-end learning of nonlinear patterns and temporal dependencies in more complex settings. Nevertheless, these methods remain series-centric and inadequately account for external drivers and task context Kim et al. [2022], Wang et al. [2024a].

**Multimodal Time-Series Forecasting.** Multimodal time series forecasting integrates external text (e.g., news and announcements) Liu et al. [2024], Dong et al. [2024] with historical numerical sequences to better capture distribution drift and structural breaks in event-driven scenarios Wang et al. [2024a]. Early approaches relied on shallow semantics such as sentiment scores or keyword, which often fail to reflect finer-grained temporal variations like mean shifts and volatility clustering. Recent advances in pretrained language models Touvron et al. [2023] have motivated direct text-series fusion via cross-attention Su et al. [2025], Liu et al. [2024] or LLMs Wang et al. [2024a], Chang et al. [2025]. However, such methods suffer from narrative redundancy and the difficulty of translating implicit, non-quantitative expressions into stable predictive signals, leading to optimization instability and performance degradation.

## 3 Preliminaries

### 3.1 Problem Formulation

We consider the multimodal time-series forecasting task. Let  $\mathbf{x}_t \in \mathbb{R}^d$  denote the numerical observation

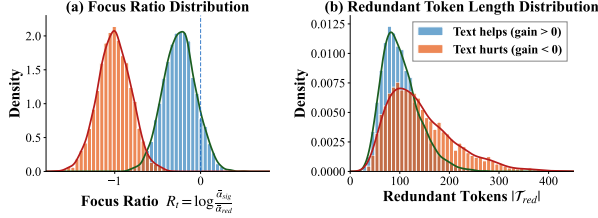


Figure 2: Analysis of attention misalignment. **Left:** Distribution of focus ratio  $R_t$  on test samples. **Right:** Relationship between redundant token count and predictive performance.

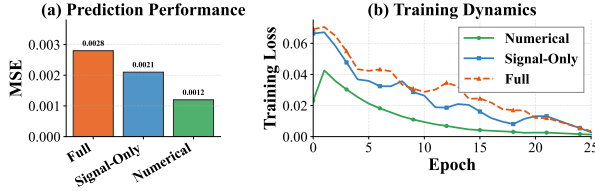


Figure 3: Comparison of three input variants. **Left:** Prediction performance (MSE) across Full, Signal-Only, and Numerical inputs. **Right:** Training loss curves showing convergence dynamics.

at time step  $t$ , and let  $s_t$  represent the temporally aligned textual information (e.g., news articles, announcements). Given a historical window of length  $L$ , the numerical input is defined as

$$\mathbf{X}_{\text{time}} = [\mathbf{x}_{t-L+1}, \dots, \mathbf{x}_t] \in \mathbb{R}^{L \times d}, \quad (1)$$

and the textual input is  $\mathbf{X}_{\text{text}} = s_t$ . The objective is to predict the numerical sequence over the next  $H$  steps:

$$\hat{\mathbf{Y}}_t = [\hat{\mathbf{x}}_{t+1}, \dots, \hat{\mathbf{x}}_{t+H}] = f_\theta(\mathbf{X}_{\text{time}}, \mathbf{X}_{\text{text}}), \quad (2)$$

where  $f_\theta$  denotes a multimodal forecasting model. The prevalent fusion paradigm employs modality-specific encoders each modality into latent representations  $\mathbf{H}_{\text{time}} = \phi_{\text{time}}(\mathbf{X}_{\text{time}}) \in \mathbb{R}^{N \times d_1}$  and  $\mathbf{H}_{\text{text}} = \phi_{\text{text}}(\mathbf{X}_{\text{text}}) \in \mathbb{R}^{M \times d_2}$ , where  $M$  is the number of text tokens, which are integrated via cross-modal attention or other fusion mechanisms.

### 3.2 Diagnosing the Modality Gap

**Semi-Synthetic Benchmark Construction** To investigate how the modality gap affects fusion, we construct a semi-synthetic benchmark where text is guaranteed to contain predictive signals, enabling controlled evaluation of information utilization. Specifically, we select FNSPID [Dong et al.,

2024], a financial dataset exhibiting pronounced non-stationarity, and extract real numerical sequences as the temporal modality input  $\mathbf{X}_{\text{time}}$ . For each sample, we further extract a set of statistical features characterizing the evolution patterns from its future window, and leverage GPT-5.2 [Singh et al., 2025] to map these features into natural language  $\mathbf{X}_{\text{text}}$  temporally aligned with the sample.

The traceable generation process enables automatic token-level annotation: tokens encoding future statistical features form the signal set  $\mathcal{T}_{\text{sig}}$ , while context-only tokens form the redundant set  $\mathcal{T}_{\text{red}}$ . Since prediction-relevant information is typically sparsely distributed within natural language, we generally have  $|\mathcal{T}_{\text{sig}}| \ll |\mathcal{T}_{\text{red}}|$ . This design preserves the naturalistic properties of text while introducing controlled interference, enabling us to quantitatively assess in a unified and interpretable setting: when text already contains effective information, whether existing fusion mechanisms can reliably localize  $\mathcal{T}_{\text{sig}}$ , suppress interference from  $\mathcal{T}_{\text{red}}$ , and genuinely translate critical semantics into predictive gains.

**Analysis of Attention Distraction** We first examine whether the fusion mechanism can correctly identify predictive signals within text. To quantify the rationality of attention allocation, we define the focus ratio:

$$R_t = \log \frac{\bar{\alpha}_{\text{sig}}}{\bar{\alpha}_{\text{red}}}, \quad (3)$$

$$\bar{\alpha}_{\text{sig}} = \frac{1}{|\mathcal{T}_{\text{sig}}|} \sum_{i \in \mathcal{T}_{\text{sig}}} \alpha_{t,i}, \quad \bar{\alpha}_{\text{red}} = \frac{1}{|\mathcal{T}_{\text{red}}|} \sum_{j \in \mathcal{T}_{\text{red}}} \alpha_{t,j},$$

Here  $\alpha_{t,i}$  denotes the cross-attention weight on token  $i$ . If the model correctly localizes predictive signals, we expect  $R_t > 0$ ; conversely,  $R_t < 0$  indicates that attention is dominated by redundant information. Figure 2 (**Left**) presents the distribution of  $R_t$  on test samples: even among samples where text yields positive predictive gains, the vast majority exhibit  $R_t < 0$ , indicating that the model systematically over-attends to redundant tokens rather than predictive signals. Figure 2 (**Right**) corroborates this finding: samples with negative gains exhibit significantly more redundant tokens, confirming that redundancy hampers textual information extraction.

**Analysis of Representational Mismatch** The preceding analysis demonstrates that redundant tokens interfere with signal extraction. A natural question arises: *if redundancy is entirely removed, can the model effectively utilize predictive information in text?* To this end, we construct three variants: FULL

(complete text), SIGNAL-ONLY (only  $\mathcal{T}_{\text{sig}}$ ), and NUMERICAL (statistical features as exogenous inputs). Figure 3 (**Left**) presents the prediction performance comparison across the three variants. SIGNAL-ONLY achieves lower MSE than FULL; however, its performance remains significantly inferior to NUMERICAL, indicating that even when redundancy is completely removed, textual signals still cannot be effectively translated into predictive gains. Figure 3 (**Right**) further corroborates this finding through training curves: NUMERICAL converges rapidly with smooth trajectories, SIGNAL-ONLY exhibits pronounced convergence lag and loss oscillation, while FULL displays the most unstable optimization dynamics. These observations collectively reveal the fundamental bottleneck of cross-modal transformation—natural language tends to characterize temporal evolution in implicit, qualitative terms (e.g., “significant rise” rather than “+15.3%”), and such semantics are difficult for existing fusion mechanisms to decode into quantitative signals usable for numerical prediction.

## 4 Methodology

As shown in Figure 4, we propose TESS, a two-stage framework built around a *Temporal Evolution Semantic Space* that distills natural language into quantifiable temporal primitives for stable cross-modal fusion. We first define this space (Section 4.1), then introduce confidence-aware text-to-primitive projection (Section 4.2), and finally present primitive-conditioned forecasting (Section 4.3).

We cast text-augmented multimodal forecasting as a semantic bottleneck: instead of directly fusing token-level features  $\mathbf{H}_{\text{text}} = \phi_{\text{text}}(\mathbf{X}_{\text{text}})$ , we compress  $\mathbf{X}_{\text{text}}$  into a compact set of temporal primitives and let the forecaster condition on these primitives together with  $\mathbf{H}_{\text{time}} = \phi_{\text{time}}(\mathbf{X}_{\text{time}})$ . Theorem 4.1 specifies when this constraint preserves predictive information and improves generalization by reducing dependence on token-level variation.

**Theorem 4.1.** *Assume semantic sufficiency (Assump. A.1) in our forecasting setting:  $\hat{\mathbf{Y}}_t \perp\!\!\!\perp \mathbf{X}_{\text{text}} \mid (\mathbf{P}_t, \mathbf{X}_{\text{time}})$ , where  $\mathbf{P}_t$  denotes the distilled primitives. Then  $\forall$  encoders  $f: \mathbf{X}_{\text{text}} \mapsto Z$ ,  $\exists$  an encoder  $\tilde{f}: \mathbf{P}_t \mapsto \tilde{Z}$  s.t.*

$$I(\tilde{Z}; \hat{\mathbf{Y}}_t \mid \mathbf{X}_{\text{time}}) = I(Z; \hat{\mathbf{Y}}_t \mid \mathbf{X}_{\text{time}}),$$

$$I(\tilde{Z}; \mathbf{X}_{\text{text}}) \leq I(Z; \mathbf{X}_{\text{text}}).$$

Moreover, under standard sub-Gaussian loss and i.i.d. sampling Assumption A.2, and A.3,

$$\text{GEN}(\tilde{Z}) \leq \text{GEN}(Z),$$

where  $\text{GEN}(\cdot)$  denotes the expected population–empirical loss gap of a predictor trained on the representation.

*Proof.* See Appendix A

### 4.1 Temporal Evolution Semantic Space

To overcome the limitations of directly mapping text to numerical sequences, we introduce an intermediate representation—the *Temporal Evolution Semantic Space*—that mediates between textual and numerical modalities. The design rationale derives from established practices in domain-specific forecasting: rather than processing descriptive details verbatim, practitioners extract implications for temporal statistical properties. Guided by this insight, we distill three categories of statistically critical features from the classical forecasting literature and formalize them as *Temporal Semantic Primitives* (TSPs). The first two primitives characterize *what* aspects of the time series evolve, while the third captures *when* and *for how long* these impacts manifest.

**(1) Distribution Shift Primitives.** Distribution shift—temporal changes in statistical properties—is identified by Kim et al. [2022] as a principal source of forecasting degradation in non-stationary time series. We characterize such shifts using two complementary primitives capturing changes in mean level and volatility. Let  $\mathbf{X}_t \in \mathbb{R}^L$  and  $\mathbf{Y}_t \in \mathbb{R}^H$  denote the observation and forecast windows. The mean shift is quantified by the standardized difference  $\Delta_\mu = (\bar{Y}_t - \bar{X}_t) / \sigma(X_t)$ , where  $\bar{X}_t = \frac{1}{L} \sum_i x_i$  and  $\bar{Y}_t = \frac{1}{H} \sum_j y_j$ .

Volatility shift is measured by  $r_\sigma = \log[(\sigma_Y + \epsilon) / (\sigma_X + \epsilon)]$ , where  $\sigma_X = \text{std}(\Delta \mathbf{X}_t)$ ,  $\sigma_Y = \text{std}(\Delta \mathbf{Y}_t)$ , and  $\Delta$  denotes the first-order differencing operator. Both shift measures are discretized using adaptive thresholds  $\tau_1 < \tau_2$  defined by training-set quantiles.

	Category	Condition	Semantics
↑↑	STRONG-RISE	$\Delta_\mu(r_\sigma) > \tau_2$	Significant increase
↑	MILD-RISE	$\tau_1 < \Delta_\mu(r_\sigma) \leq \tau_2$	Moderate increase
—	STABLE	$-\tau_1 \leq \Delta_\mu(r_\sigma) \leq \tau_1$	Level unchanged
↓	MILD-DROP	$-\tau_2 \leq \Delta_\mu(r_\sigma) < -\tau_1$	Moderate decrease
↓↓	STRONG-DROP	$\Delta_\mu(r_\sigma) < -\tau_2$	Significant decrease

**(2) Shape Primitive  $p_{\text{shape}}$ .** Nie et al. [2023] demonstrate that patch-level morphology conveys rich predictive information. The shape primitive encodes the *inter-patch trend sequence* to characterize internal evolution structure. Concretely, we partition  $\mathbf{Y}_t = (y_1, \dots, y_H)$  into  $N_{\text{fcst}}$  equally-sized patches

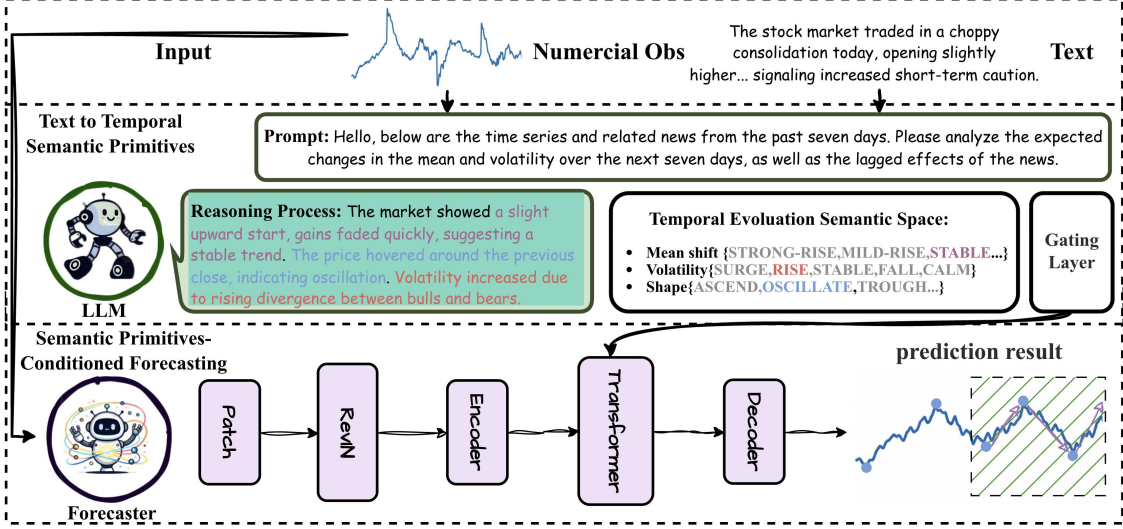


Figure 4: Overview of TESS. Given numerical observations and associated text, a frozen LLM extracts temporal evolution primitives (e.g., mean shift, shape, volatility, lag) via structured prompting. These primitives, after confidence-aware gating, condition a Transformer-based forecaster that fuses semantic signals with encoded historical sequences to produce numerical predictions.

of length  $L_u = H/N_{\text{fcst}}$ . For each patch  $i$ , we compute its mean  $\bar{u}_i = \frac{1}{L_u} \sum_{j=(i-1)L_u+1}^{iL_u} y_j$  and define inter-patch trend signs  $s_i = \text{sgn}_\tau(\bar{u}_{i+1} - \bar{u}_i)$ , where  $\text{sgn}_\tau(x) = +1$  if  $x > \tau$ ,  $-1$  if  $x < -\tau$ , and  $0$  otherwise. The dominant pattern of  $(s_1, \dots, s_{N_{\text{fcst}}-1})$  determines the shape category:

Category	Condition	Semantics
	ASCEND $\forall i: s_i \geq 0 \wedge \exists i: s_i = +1$	Sustained uptrend
	DESCEND $\forall i: s_i \leq 0 \wedge \exists i: s_i = -1$	Sustained downtrend
	PEAK rise-then-fall with sign changes	Rise then fall
	TROUGH fall-then-rise with sign changes	Fall then rise
	OSCILLATE multiple sign reversals	Fluctuating

(3) **Lag and Decay Primitive  $p_{\text{lag}}$ .** The same mean increase or volatility surge may exhibit vastly different response dynamics (transient pulse vs. long-tailed decay). Inspired by distributed-lag models and impulse response functions [Yang et al., 2024], we propose the lag-and-decay primitive to localize influence timing and persistence within the forecast horizon. Using the same patch partition, we compute influence intensity for each patch:  $a_i = |(\bar{u}_i - \bar{X}_t)/\sigma(X_t) + \alpha| \log((\sigma(\Delta \mathbf{u}_i) + \epsilon)/(\sigma(\Delta \mathbf{X}_t) + \epsilon))$ , and normalize to obtain an influence distribution  $\pi_i = a_i / \sum_j a_j$ . We then derive three indicators: (i) centroid  $c = \sum_i \pi_i \cdot (i-1)/(N_{\text{fcst}}-1) \in [0, 1]$ , where smaller  $c$  indicates earlier onset; (ii) tail mass  $d = \sum_{i>i^*} \pi_i$  (with  $i^* = \arg \max_i \pi_i$ ), where larger  $d$  indicates stronger persistence; (iii) peak prominence  $q = \max_i \pi_i$ , distinguishing concentrated from diffuse effects. Given thresholds  $\kappa_1 < \kappa_2$  (timing),  $\rho$

(persistence), and  $\eta$  (prominence):

Category	Condition	Semantics
	EARLY-FADE $q > \eta, c \leq \kappa_1, d \leq \rho$	Early onset, quick decay
	EARLY-PERSIST $q > \eta, c \leq \kappa_1, d > \rho$	Early onset, persistent
	MID-FADE $q > \eta, \kappa_1 < c \leq \kappa_2, d \leq \rho$	Mid-horizon pulse
	MID-PERSIST $q > \eta, \kappa_1 < c \leq \kappa_2, d > \rho$	Mid-horizon, persistent
	LATE $q > \eta, c > \kappa_2$	Late manifestation
	DIFFUSE $q \leq \eta$	Distributed impact

The above design ensures that each primitive  $p_k$  possesses *numerical verifiability*: given observation and forecast sequences, the ground-truth value  $v_{t,k}$  is uniquely determined via  $\psi_k$ , thereby furnishing reliable supervision for the gating mechanism. All thresholds are set adaptively based on training-set statistics (e.g., quantiles).

## 4.2 Text to Temporal Semantic Primitives

This stage describes how to reliably predict the discrete value of each semantic primitive  $p_k$  from textual input  $s_t$ , and estimate its confidence to filter noisy extractions.

**LLM-based Primitive Classification.** Given the finite value domain  $\mathcal{V}_k$  of each primitive, we formulate extraction as multi-class classification using a frozen LLM as the classifier. Under a structured prompt  $\mathcal{D}_k$  (containing primitive semantic definitions and representative examples), we compute

log-likelihood scores for each candidate  $v \in \mathcal{V}_k$ :

$$\ell_{t,k}(v) = \log P_{\text{LLM}}(v \mid s_t, \mathcal{D}_k). \quad (4)$$

Applying temperature-scaled softmax yields a categorical distribution and the predicted class:

$$q_{t,k}(v) = \frac{\exp(\ell_{t,k}(v)/T)}{\sum_{v' \in \mathcal{V}_k} \exp(\ell_{t,k}(v')/T)}, \quad (5)$$

$$\hat{v}_{t,k} = \arg \max_{v \in \mathcal{V}_k} q_{t,k}(v), \quad (6)$$

where  $T$  is a temperature coefficient. This procedure yields both the discrete prediction  $\hat{v}_{t,k}$  and the full distribution  $q_{t,k}(\cdot)$ , which provides calibration signals for subsequent confidence estimation.

**Confidence-Aware Gating.** Although LLMs can discriminate based on primitive definitions, real-world text often contains narrative noise and ambiguous expressions that may lead to extraction errors. To mitigate the negative impact of erroneous primitives on downstream predictions [Wang et al., 2025a], we introduce a confidence gate  $g_{t,k} \in [0, 1]$  for each primitive to suppress unreliable semantic injection during inference.

Since each primitive’s candidate set  $\mathcal{V}_k$  is small, we adopt a simple uncertainty indicator as the calibration signal: the log-probability margin between the top-1 and top-2 candidates. Let  $v^{(1)}, v^{(2)}$  denote the classes with highest and second-highest probability under  $q_{t,k}(\cdot)$ :

$$m_{t,k} = \log q_{t,k}(v^{(1)}) - \log q_{t,k}(v^{(2)}). \quad (7)$$

We map the predicted class  $\hat{v}_{t,k}$  to an internal semantic vector  $\mathbf{h}_{t,k}$  via a learnable embedding matrix  $\mathbf{E}_k \in \mathbb{R}^{|\mathcal{V}_k| \times d}$ :

$$\mathbf{h}_{t,k} = \mathbf{E}_k[\hat{v}_{t,k}], \quad (8)$$

where each row of  $\mathbf{E}_k$  corresponds to one discrete class of primitive  $k$ , learned end-to-end with the downstream predictor. The gating network fuses the semantic embedding with the margin to estimate confidence:

$$g_{t,k} = \sigma(\mathbf{w}_k^\top [\mathbf{h}_{t,k}; \mathbf{W}_m m_{t,k}] + b_k), \quad (9)$$

where  $\mathbf{W}_m \in \mathbb{R}^d$  projects the scalar margin to the embedding dimension. Thanks to the numerical ground-truth labels from the forecast window  $v_{t,k}^* = \psi_k(\mathbf{Y}_t)$  and construct supervision labels  $y_{t,k} = \mathcal{K}[\hat{v}_{t,k} = v_{t,k}^*]$ . The gating network is trained with binary cross-entropy:

$$\mathcal{L}_{\text{gate}} = - \sum_{t,k} [y_{t,k} \log g_{t,k} + (1 - y_{t,k}) \log(1 - g_{t,k})]. \quad (10)$$

During inference, we apply soft weighting  $\tilde{\mathbf{h}}_{t,k} = g_{t,k} \cdot \mathbf{h}_{t,k}$ , allowing high-confidence primitives to dominate predictions while suppressing interference from erroneous extractions.

### 4.3 Semantic Primitives-Conditioned Forecasting

We feed the gated primitives  $\tilde{h}_{t,k} = g_{t,k} h_{t,k}$  into the forecaster to produce  $\hat{y}_t$ . Under a mild Lipschitz assumption on the forecaster, the error induced by an incorrect primitive is attenuated on the order of  $g_{t,k}^2$  (Theorem A.5). We adopt PatchTST Nie et al. [2023] as the backbone architecture and introduce a semantic conditioning mechanism.

**Time-Series Encoding.** Following PatchTST [Nie et al., 2023], we first apply instance normalization [Kim et al., 2022] to the input sequence  $\mathbf{x} \in \mathbb{R}^L$  to mitigate distribution shift between training and testing: for each instance we compute mean  $\mu$  and standard deviation  $s$ , then normalize before patching. The input is segmented into  $N = \lfloor (L - P)/S \rfloor + 1$  patches, where  $P$  is the patch length and  $S$  is the stride. Each patch is mapped to the  $d$ -dimensional latent space via a trainable linear projection  $\mathbf{W}_p \in \mathbb{R}^{d \times P}$ , with learnable positional encodings  $\mathbf{W}_{\text{pos}} \in \mathbb{R}^{d \times N}$  added to obtain patch embeddings  $\mathbf{E}_{\text{patch}} \in \mathbb{R}^{N \times d}$ .

**Semantic Primitives-Conditioned Prediction.** The  $K$  gated semantic vectors  $\tilde{\mathbf{h}}_{t,k} \in \mathbb{R}^d$  from Section 4.2 are stacked to form semantic prefix tokens  $\mathbf{P} \in \mathbb{R}^{K \times d}$ , concatenated with patch embeddings to form the Transformer input:

$$\mathbf{Z}^{(0)} = [\mathbf{P}; \mathbf{E}_{\text{patch}}] \in \mathbb{R}^{(K+N) \times d}. \quad (11)$$

The input sequence is processed by  $M$  Transformer encoder layers. Each layer first captures sequential dependencies via  $H$ -head self-attention:

$$\text{Attn}(\mathbf{Q}, \mathbf{K}, \mathbf{V}) = \text{Softmax} \left( \frac{\mathbf{Q}\mathbf{K}^\top}{\sqrt{d/H}} \right) \mathbf{V}, \quad (12)$$

where  $\mathbf{Q}, \mathbf{K}, \mathbf{V} \in \mathbb{R}^{(K+N) \times (d/H)}$  are obtained via linear projections. Multi-head outputs are concatenated and updated through feed-forward networks with residual connections. This prefix fusion allows semantic information to participate in temporal modeling throughout the attention mechanism. Finally, we extract patch-corresponding outputs  $\mathbf{Z}_{\text{out}} \in \mathbb{R}^{N \times d}$ , flatten and map to the forecast horizon via an MLP,

and apply inverse normalization to recover the original scale:

$$\hat{\mathbf{y}} = s \cdot \text{MLP}(\text{Flatten}(\mathbf{Z}_{\text{out}})) + \mu \in \mathbb{R}^H. \quad (13)$$

**Training Objective.** The model is trained end-to-end (with the LLM frozen) using MSE loss to measure prediction-target discrepancy, jointly optimized with gating supervision:

$$\mathcal{L} = \mathcal{L}_{\text{fcst}} + \lambda \mathcal{L}_{\text{gate}}, \quad \mathcal{L}_{\text{fcst}} = \frac{1}{H} \|\hat{\mathbf{y}} - \mathbf{y}\|_2^2. \quad (14)$$

## 5 Experiments

### 5.1 Experimental Setup

**Benchmark.** We evaluate TESS on four real-world datasets spanning financial and general domains. **Financial time-series datasets** include FNSPID [Dong et al., 2024] and Bitcoin, both exhibiting significant event-driven non-stationarity. **General time-series datasets** include Electricity and Environment, used to verify cross-domain generalization. For all datasets, we strictly follow the standard evaluation protocols and official data splits from the original literature to ensure fair comparison and reproducibility. Detailed dataset statistics are provided in Appendix B.

**Baselines.** We compare TESS against two categories of baselines: **(i) Unimodal time-series models**, including TimeMixer [Wang et al., 2024b], TSMixer [Chen et al., 2023], Nonstationary Transformer [Liu et al., 2022b], TimesNet [Wu et al., 2023], FEDformer [Zhou et al., 2022], Pyraformer [Liu et al., 2022a], Reformer [Kitaev et al., 2020], and PatchTST [Nie et al., 2023], covering mainstream architectures such as MLP and Transformer variants, all implemented using Time-Series-Library<sup>1</sup>; **(ii) Multimodal fusion models**, including TimeLLM [Jin et al., 2024], ChatTime [Wang et al., 2025b], and NewsForecasting [Wang et al., 2024a], all using official implementations. Hyperparameters for all baselines are determined via grid search on the validation set to ensure fair comparison. Detailed baseline configurations are provided in Appendix C.

**Implementation Details.** We implement all experiments in PyTorch [Paszke et al., 2019] on 8 NVIDIA A100 80GB GPUs, using AdamW [Loshchilov and Hutter, 2017] with learning rate  $\in \{1e-4, 5e-4, 1e-3\}$  and early stopping (patience=10) on validation loss.

<sup>1</sup><https://github.com/thuml/Time-Series-Library>

### 5.2 Main Results

Table 1 presents the performance comparison between TESS and all baselines across four datasets. **(i) Significant improvements on financial datasets.** On financial datasets exhibiting pronounced non-stationarity (FNSPID and Bitcoin), TESS achieves substantial performance gains. Specifically, on FNSPID, TESS improves over the strongest baseline TimesNet by 3.3%, 20.0%, and 9.9% across three metrics. On Bitcoin, TESS outperforms the strongest baseline NewsForecasting by 18.2%, 29.1%, and 15.8% in terms of MAE, MSE, and RMSE, respectively. These results demonstrate the superiority of the temporal evolution semantic space in capturing event-driven non-stationary dynamics. **(ii) Stable performance on general datasets.** On general datasets, TESS likewise demonstrates competitive performance. On Electricity, TESS achieves the best performance across all metrics, improving over the strongest baseline by 0.4%–5.0%. On Environment, TESS attains runner-up performance with less than 1% gap from the strongest baseline Nonstationary Transformer. These results indicate that TESS maintains stable predictive capability even in scenarios with relatively mild non-stationarity.

#### Effectiveness in Non-Stationary Scenarios.

To further validate TESS’s performance under different non-stationarity patterns, we extract three subsets from the test set, each representing a non-stationary scenario: **(i) Shape transition**, **(ii) Volatility change**, and **(iii) Mean shift**. Figure 5 presents the MSE performance across different methods. TESS achieves consistent improvements across all three non-stationary scenarios, with MSE reductions of 21–52% over multimodal baselines and 21–45% over unimodal baselines on FNSPID and Bitcoin.

### 5.3 Model Analysis

**Ablation Study.** We ablate TESS and the gating mechanism on three datasets. Since gating relies on primitives extracted by TESS, removing TESS necessarily entails removing gating as well. Table 2 presents the results. Removing TESS leads to substantial degradation, with MSE increasing by 46.2%, 29.4%, and 22.8% respectively, confirming its effectiveness. In contrast, removing gating incurs more modest increases of 3.7%, 2.6%, and 7.5%, indicating that confidence-aware gating effectively filters extraction errors. These results underscore the necessity of both components: TESS drives performance

Table 1: Comparison of baselines for time-series forecasting. Lower scores indicate better performance. **Red**: best, **Blue**: runner-up.

Model	Bitcoin (Finance)			FNSPID (Finance)			Electricity (General)			Environment (General)		
	MAE	MSE	RMSE	MAE	MSE	RMSE	MAE	MSE	RMSE	MAE	MSE	RMSE
<b>Traditional Models</b>												
TimeMixer	1.6757	4.3725	2.0910	0.0153	0.0017	0.0407	0.1064	0.0252	0.1586	0.4219	0.3693	0.6077
TSMixer	4.1202	29.1934	5.4031	0.0353	0.0082	0.0907	0.1119	0.0258	0.1606	0.4860	0.3878	0.6227
Nonstationary	1.6003	4.3420	2.0837	0.0154	0.0016	0.0400	0.1066	0.0256	0.1600	<b>0.4178</b>	<b>0.3472</b>	<b>0.5892</b>
TimesNet	1.4598	3.8229	1.9552	<b>0.0152</b>	<b>0.0015</b>	0.0385	0.1035	<b>0.0242</b>	<b>0.1557</b>	0.4258	0.3473	<b>0.5893</b>
FEDformer	1.4197	3.2768	1.8102	0.0163	0.0016	0.0396	0.1144	0.0267	0.1633	0.4513	0.3650	0.5893
Pyraformer	1.3994	3.6377	1.9073	0.0168	0.0015	<b>0.0383</b>	0.1117	0.0261	0.1616	0.4303	0.3649	0.6041
Reformer	12.4630	157.8843	12.5652	0.0299	0.0141	0.1188	0.1180	0.0292	0.1709	0.4258	0.3473	0.5893
PatchTST	1.3615	3.2456	1.8016	0.0160	0.0016	0.0402	<b>0.1047</b>	0.0243	0.1559	0.4290	0.3706	0.6088
<b>Multimodal Models</b>												
TimeLLM	1.3940	3.4477	1.8568	0.0158	0.0017	0.0412	0.1074	0.0255	0.1596	0.4237	0.3714	0.6094
ChatTime	1.4774	3.9389	1.9846	0.0187	0.0018	0.0424	0.1149	0.0279	0.1670	0.4344	0.3787	0.6153
NewsForecasting	<b>1.3593</b>	<b>3.2036</b>	<b>1.7898</b>	0.0176	0.0017	0.0412	0.1088	0.0254	0.1593	0.4378	0.3678	0.6064
Ours	<b>1.1120</b>	<b>2.2726</b>	<b>1.5075</b>	<b>0.0147</b>	<b>0.0012</b>	<b>0.0347</b>	<b>0.1031</b>	<b>0.0230</b>	<b>0.1518</b>	<b>0.4202</b>	<b>0.3534</b>	0.5945
Gain vs. best (%)	+18.2%	+29.1%	+15.8%	+3.3%	+20.0%	+9.9%	+0.4%	+5.0%	+2.5%	-0.6%	-1.8%	-0.9%

Table 2: Ablation study on the contributions of temporal evolution semantic space (TESS) and gating mechanism. Lower scores indicate better performance. **Red**: best performance.

Dataset	Metric	w/o TESS	w/o Gating	TESS
Bitcoin	MAE	1.6025	1.1532	<b>1.1120</b>
	MSE	4.2238	2.3556	<b>2.2726</b>
	RMSE	2.0552	1.5349	<b>1.5075</b>
FNSPID	MAE	0.0155	0.0151	<b>0.0147</b>
	MSE	0.0018	0.0015	<b>0.0012</b>
	RMSE	0.0412	0.0387	<b>0.0347</b>
Electricity	MAE	0.1214	0.1070	<b>0.1031</b>
	MSE	0.0298	0.0248	<b>0.0230</b>
	RMSE	0.1726	0.1575	<b>0.1518</b>

gains, while gating enhances robustness against LLM extraction errors.

**Case Study** Figure 7 illustrates four representative prediction cases. On Bitcoin, TESS successfully captures mean shift and trend patterns (e.g., MILD-RISE, TROUGH); on Electricity, it identifies shape transitions with appropriate temporal localization (e.g., MID-FADE, LATE). In contrast, direct text fusion fails to capture these patterns, leading to substantial prediction deviations. These results confirm that the semantic space effectively bridges implicit textual signals and quantifiable forecasting gains.

**Effectiveness of Temporal Evolution Semantic Space.** First, Figure 6 shows that TESS exhibits

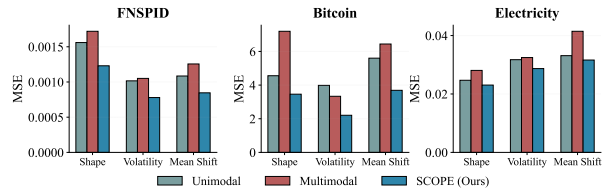


Figure 5: Performance comparison on three types of non-stationary scenarios (Shape, Volatility, Mean Shift). TESS (blue) consistently outperforms both unimodal (teal) and multimodal (red) baselines.

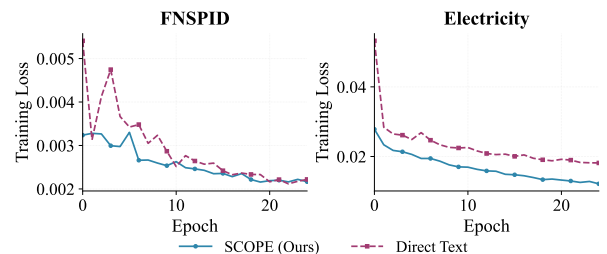


Figure 6: Training loss curves comparison. TESS (blue) converges faster with smoother dynamics than direct text fusion (purple).

faster and smoother convergence than direct text fusion on both FNSPID and Electricity, indicating that the semantic space alleviates cross-modal optimization challenges. Second, Figure 8(a) presents

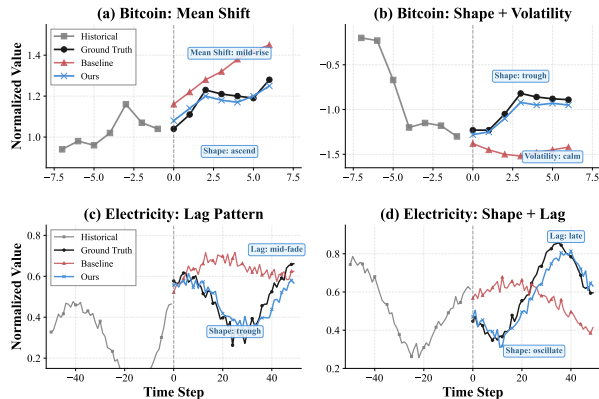


Figure 7: Case study on Bitcoin and Electricity datasets. TESS (blue) accurately captures temporal evolution primitives and aligns closely with ground truth (black).

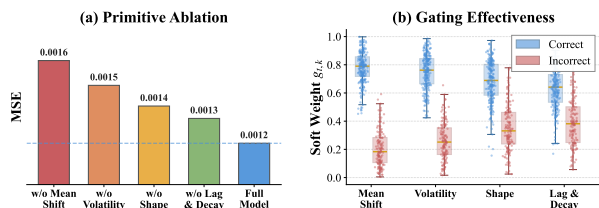


Figure 8: Analysis of temporal evolution semantic space. (a) Primitive ablation on FNSPID: removing each primitive leads to MSE increase, with Mean Shift having the largest impact. (b) Gating effectiveness: correctly extracted primitives (blue) receive significantly higher soft weights than incorrect ones (red).

primitive ablation on FNSPID: removing Mean Shift alone increases MSE by 33%, underscoring its role in capturing non-stationarity; removing other primitives also incurs performance loss. Best performance is achieved when all four primitives are jointly used, confirming their complementarity.

**Effectiveness of Gating Mechanism.** Figure 8(b) presents the soft weight distributions across the four primitives on the FNSPID dataset. The results demonstrate that gating weights are highly correlated with primitive correctness: correctly extracted samples exhibit median weights predominantly in the range of 0.65–0.78, whereas incorrectly extracted samples show median weights of only 0.21–0.40. This indicates that the gating network successfully learns to map the uncertainty signals from LLM outputs to reliability estimates, sup-

pressing the interference of erroneous primitives on predictions through soft weighting.

## 6 Conclusion

We propose TESS, a two-stage framework that bridges text-numerical modality gaps through a Temporal Evolution Semantic Space. A confidence-aware gating mechanism further ensures robustness against LLM extraction errors. Extensive experiments across financial and general domains demonstrate that TESS achieves up to 29% MSE reduction over state-of-the-art methods.

## Impact Statement

This paper presents work whose goal is to advance the field of time series analysis and multi model forecasting. There are many potential societal consequences of our work, none which we feel must be specifically highlighted here.

## References

- Yang An, Zhibin Li, Xiaoyu Li, Wei Liu, Xinghao Yang, Haoliang Sun, Meng Chen, Yu Zheng, and Yongshun Gong. Spatio-temporal multivariate probabilistic modeling for traffic prediction. *IEEE Transactions on Knowledge and Data Engineering*, 37(5):2986–3000, 2025. doi: 10.1109/TKDE.2025.3539680.
- Ching Chang, Jeehyun Hwang, Yidan Shi, Haixin Wang, Wen-Chih Peng, Tien-Fu Chen, and Wei Wang. Time-imm: A dataset and benchmark for irregular multimodal multivariate time series. *arXiv preprint arXiv:2506.10412*, 2025.
- Bo-Juen Chen, Ming-Wei Chang, et al. Load forecasting using support vector machines: A study on eunite competition 2001. *IEEE transactions on power systems*, 19(4):1821–1830, 2004.
- Si-An Chen, Chun-Liang Li, Sercan O Arik, Nathanael Christian Yoder, and Tomas Pfister. TSMixer: An all-MLP architecture for time series forecasting. *Transactions on Machine Learning Research*, 2023. ISSN 2835-8856. URL <https://openreview.net/forum?id=wbpxTuXgm0>.
- Jinliang Deng, Xiushi Chen, Renhe Jiang, Du Yin, Yi Yang, Xuan Song, and Ivor W Tsang. Disentangling structured components: Towards adaptive, interpretable and scalable time series forecasting.

- IEEE Transactions on Knowledge and Data Engineering*, 36(8):3783–3800, 2024.
- Zihan Dong, Xinyu Fan, and Zhiyuan Peng. Fnspid: A comprehensive financial news dataset in time series. In *Proceedings of the 30th ACM SIGKDD Conference on Knowledge Discovery and Data Mining*, pages 4918–4927, 2024.
- Yuntao Du, Jindong Wang, Wenjie Feng, Sinno Pan, Tao Qin, Renjun Xu, and Chongjun Wang. Adarnn: Adaptive learning and forecasting of time series. In *Proceedings of the 30th ACM International Conference on Information & Knowledge Management*, pages 402–411, 2021.
- Shyh-Jier Huang and Kuang-Rong Shih. Short-term load forecasting via arma model identification including non-gaussian process considerations. *IEEE Transactions on power systems*, 18(2):673–679, 2003.
- Ming Jin, Shiyu Wang, Lintao Ma, Zhixuan Chu, James Y. Zhang, Xiaoming Shi, Pin-Yu Chen, Yuxuan Liang, Yuan-Fang Li, Shirui Pan, and Qingsong Wen. Time-LLM: Time series forecasting by reprogramming large language models. In *The Twelfth International Conference on Learning Representations*, 2024. URL <https://openreview.net/forum?id=Unb5CVPtAE>.
- Prajakta S Kalekar et al. Time series forecasting using holt-winters exponential smoothing. *Kanwal Rekhi school of information Technology*, 4329008(13):1–13, 2004.
- HyunGi Kim, Siwon Kim, Jisoo Mok, and Sungroh Yoon. Battling the non-stationarity in time series forecasting via test-time adaptation. In *Proceedings of the AAAI Conference on Artificial Intelligence*, volume 39, pages 17868–17876, 2025.
- Taesung Kim, Jinhee Kim, Yunwon Tae, Cheonbok Park, Jang-Hyun Choo, and Junmo Ko. Reversible instance normalization for accurate time-series forecasting against distribution shift. In *International Conference on Learning Representations*, 2022.
- Nikita Kitaev, Lukasz Kaiser, and Anselm Levskaya. Reformer: The efficient transformer. In *International Conference on Learning Representations*, 2020. URL <https://openreview.net/forum?id=rkgNkkHtvB>.
- Ross Koval, Nicholas Andrews, and Xifeng Yan. Multimodal language models for financial forecasting from interleaved sequences of text and time series. In *Proceedings of the 14th International Joint Conference on Natural Language Processing and the 4th Conference of the Asia-Pacific Chapter of the Association for Computational Linguistics*, pages 987–1001, 2025.
- Victor Weixin Liang, Yuhui Zhang, Yongchan Kwon, Serena Yeung, and James Y Zou. Mind the gap: Understanding the modality gap in multi-modal contrastive representation learning. *Advances in Neural Information Processing Systems*, 35:17612–17625, 2022.
- Haoxin Liu, Shangqing Xu, Zhiyuan Zhao, Lingkai Kong, Harshavardhan Prabhakar Kamarthi, Aditya Sasanur, Megha Sharma, Jiaming Cui, Qingsong Wen, Chao Zhang, et al. Time-mmd: Multi-domain multimodal dataset for time series analysis. *Advances in Neural Information Processing Systems*, 37:77888–77933, 2024.
- Shizhan Liu, Hang Yu, Cong Liao, Jianguo Li, Weiyao Lin, Alex X Liu, and Schahram Dustdar. Pyraformer: Low-complexity pyramidal attention for long-range time series modeling and forecasting. In *# PLACEHOLDER\_PARENT\_METADATA\_VALUE#*, 2022a.
- Yong Liu, Haixu Wu, Jianmin Wang, and Mingsheng Long. Non-stationary transformers: Exploring the stationarity in time series forecasting. *Advances in neural information processing systems*, 35:9881–9893, 2022b.
- Ilya Loshchilov and Frank Hutter. Decoupled weight decay regularization. *arXiv preprint arXiv:1711.05101*, 2017.
- Yuqi Nie, Nam H Nguyen, Phanwadee Sinthong, and Jayant Kalagnanam. A time series is worth 64 words: Long-term forecasting with transformers. In *The Eleventh International Conference on Learning Representations*, 2023. URL <https://openreview.net/forum?id=Jbdc0vT0col>.
- Hao Niu, Yun Xiong, Xiaosu Wang, Wenjing Yu, Yao Zhang, and Weizu Yang. Kefvp: Knowledge-enhanced financial volatility prediction. In *Findings of the Association for Computational Linguistics: EMNLP 2023*, pages 11499–11513, 2023.
- Takayuki Osogami. Second order techniques for learning time-series with structural breaks. In *Proceedings of the AAAI Conference on Artificial Intelligence*, volume 35, pages 9259–9267, 2021.

- Adam Paszke, Sam Gross, Francisco Massa, Adam Lerer, James Bradbury, Gregory Chanan, Trevor Killeen, Zeming Lin, Natalia Gimelshein, Luca Antiga, et al. Pytorch: An imperative style, high-performance deep learning library. *Advances in neural information processing systems*, 32, 2019.
- Ramit Sawhney, Shivam Agarwal, Arnav Wadhwa, and Rajiv Shah. Deep attentive learning for stock movement prediction from social media text and company correlations. In *Proceedings of the 2020 conference on empirical methods in natural language processing (EMNLP)*, pages 8415–8426, 2020.
- Aaditya Singh, Adam Fry, Adam Perelman, Adam Tart, Adi Ganesh, Ahmed El-Kishky, Aidan McLaughlin, Aiden Low, AJ Ostrow, Akhila Ananthram, et al. Openai gpt-5 system card. *arXiv preprint arXiv:2601.03267*, 2025.
- Chen Su, Yuanhe Tian, Yan Song, and Yongdong Zhang. Text reinforcement for multimodal time series forecasting, 2025. URL <https://arxiv.org/abs/2509.00687>.
- Hugo Touvron, Thibaut Lavril, Gautier Izacard, Xavier Martinet, Marie-Anne Lachaux, Timothée Lacroix, Baptiste Rozière, Naman Goyal, Eric Hambro, Faisal Azhar, et al. Llama: Open and efficient foundation language models. *arXiv preprint arXiv:2302.13971*, 2023.
- Bin Wang, Yongqi Han, Minbo Ma, Tianrui Li, Junbo Zhang, Feng Hong, and Yanwei Yu. Non-collective calibrating strategy for time series forecasting. In *Proceedings of the Thirty-Fourth International Joint Conference on Artificial Intelligence, IJCAI '25*, 2025a. ISBN 978-1-956792-06-5. doi: 10.24963/ijcai.2025/371. URL <https://doi.org/10.24963/ijcai.2025/371>.
- Chengsen Wang, Qi Qi, Jingyu Wang, Haifeng Sun, Zirui Zhuang, Jinming Wu, Lei Zhang, and Jianxin Liao. Chattime: A unified multimodal time series foundation model bridging numerical and textual data. In *Proceedings of the AAAI Conference on Artificial Intelligence*, volume 39, pages 12694–12702, 2025b.
- Xinlei Wang, Maike Feng, Jing Qiu, Jinjin Gu, and Junhua Zhao. From news to forecast: Integrating event analysis in llm-based time series forecasting with reflection. *Advances in Neural Information Processing Systems*, 37:58118–58153, 2024a.
- Yuxuan Wang, Haixu Wu, Jiayang Dong, Guo Qin, Haoran Zhang, Yong Liu, Yunzhong Qiu, Jianmin Wang, and Mingsheng Long. Timexer: Empowering transformers for time series forecasting with exogenous variables. *Advances in Neural Information Processing Systems*, 37:469–498, 2024b.
- Haixu Wu, Jiehui Xu, Jianmin Wang, and Mingsheng Long. Autoformer: Decomposition transformers with auto-correlation for long-term series forecasting. *Advances in neural information processing systems*, 34:22419–22430, 2021.
- Haixu Wu, Tengge Hu, Yong Liu, Hang Zhou, Jianmin Wang, and Mingsheng Long. Timesnet: Temporal 2d-variation modeling for general time series analysis. In *International Conference on Learning Representations*, 2023.
- Aolin Xu and Maxim Raginsky. Information-theoretic analysis of generalization capability of learning algorithms. In *Advances in Neural Information Processing Systems*, volume 30, 2017.
- Min Yang, Yang An, Jinliang Deng, Xiaoyu Li, Bin Xu, Ji Zhong, Xiankai Lu, and Yongshun Gong. Can-st: Clustering adaptive normalization for spatio-temporal ood learning. In *Proceedings of the Thirty-Fourth International Joint Conference on Artificial Intelligence*, pages 3543–3551, 2025.
- Yingnan Yang, Qingling Zhu, and Jianyong Chen. Vcformer: Variable correlation transformer with inherent lagged correlation for multivariate time series forecasting. In *Proceedings of the Thirty-Third International Joint Conference on Artificial Intelligence*, pages 5335–5343, 2024. URL <https://www.ijcai.org/proceedings/2024/590>.
- Ailing Zeng, Muxi Chen, Lei Zhang, and Qiang Xu. Are transformers effective for time series forecasting? In *Proceedings of the AAAI conference on artificial intelligence*, volume 37, pages 11121–11128, 2023.
- Haoyi Zhou, Shanghang Zhang, Jieqi Peng, Shuai Zhang, Jianxin Li, Hui Xiong, and Wancai Zhang. Informer: Beyond efficient transformer for long sequence time-series forecasting. In *Proceedings of the AAAI conference on artificial intelligence*, volume 35, pages 11106–11115, 2021.
- Tian Zhou, Ziqing Ma, Qingsong Wen, Xue Wang, Liang Sun, and Rong Jin. Fedformer: Frequency enhanced decomposed transformer for long-term series forecasting. In *International conference on machine learning*, pages 27268–27286. PMLR, 2022.

## A Theorems & Proofs

Throughout this section, we write  $(X, S, Y) := (\mathbf{X}_{\text{text}}, \mathbf{X}_{\text{time}}, \hat{\mathbf{Y}}_t)$  and  $V := \phi(X)$ .

Let  $\mathcal{S} = \{(X_i, Y_i)\}_{i=1}^n \sim p(x, y)^{\otimes n}$ . Given an encoder  $p(z | x)$ , draw  $Z_i \sim p(\cdot | X_i)$  independently and let  $Z = (Z_1, \dots, Z_n)$ . Define

$$L_{\text{POP}}(Z) := \mathbb{E}[\ell(Z, Y)], \quad L_{\text{EMP}}(Z) := \frac{1}{n} \sum_{i=1}^n \ell(Z_i, Y_i).$$

**Assumption A.1.**  $Y \perp X | (V, S)$  (i.e.,  $p(y | x, s) = p(y | v, s)$  for  $v = \phi(x)$ ).

**Assumption A.2.**  $\ell(Z, y)$  is  $\sigma$ -sub-Gaussian under  $Z \sim p(\cdot | x)$  for all  $(x, y)$ .

**Assumption A.3.** Conditioned on  $\mathcal{S}$ ,  $Z_i \perp Z_j$  for  $i \neq j$ ; hence  $I(Z; \mathcal{S}) = \sum_{i=1}^n I(Z_i; X_i) = n I(Z; X)$ .

*Theorem* (Restatement of Theorem 4.1). Assume semantic sufficiency (Assump. A.1) in our forecasting setting:  $\hat{\mathbf{Y}}_t \perp\!\!\!\perp \mathbf{X}_{\text{text}} | (\mathbf{P}_t, \mathbf{X}_{\text{time}})$ , where  $\mathbf{P}_t$  denotes the distilled primitives. Then  $\forall$  encoders  $f : \mathbf{X}_{\text{text}} \mapsto Z$ ,  $\exists$  an encoder  $\tilde{f} : \mathbf{P}_t \mapsto \tilde{Z}$  s.t.

$$\begin{aligned} I(\tilde{Z}; \hat{\mathbf{Y}}_t | \mathbf{X}_{\text{time}}) &= I(Z; \hat{\mathbf{Y}}_t | \mathbf{X}_{\text{time}}), \\ I(\tilde{Z}; \mathbf{X}_{\text{text}}) &\leq I(Z; \mathbf{X}_{\text{text}}). \end{aligned}$$

Moreover, under standard sub-Gaussian loss and i.i.d. sampling Assumption A.2, and A.3,

$$\text{GEN}(\tilde{Z}) \leq \text{GEN}(Z),$$

where  $\text{GEN}(\cdot)$  denotes the expected population–empirical loss gap of a predictor trained on the representation.

*Proof.* We use  $p$  to denote both the data law  $p(x, s, y)$  and the original encoder  $p(z | x)$ . The induced joint on  $(X, S, Y, Z)$  factorizes as

$$p(x, s, y, z) = p(z | x) p(y | x, s) p(x, s),$$

since  $Z \perp (Y, S) | X$ . Define

$$I_p(Z; Y | S) := \sum_s p(s) \sum_{z, y} p(z, y | s) \log \frac{p(z, y | s)}{p(z | s) p(y | s)}, \quad (15)$$

$$I_p(Z; X) := \sum_x p(x) \sum_z p(z | x) \log \frac{p(z | x)}{p(z)}. \quad (16)$$

Let  $V = \phi(X)$ . Define

$$p(v, s) := \sum_{x: \phi(x)=v} p(x, s), \quad \alpha_{x|v, s} := \frac{p(x, s)}{p(v, s)} \quad (\phi(x) = v),$$

so  $\sum_{x: \phi(x)=v} \alpha_{x|v, s} = 1$ . Then set

$$p(z | v, s) := \sum_{x: \phi(x)=v} \alpha_{x|v, s} p(z | x), \quad (17)$$

which is a valid conditional distribution. Define the new encoder

$$\tilde{p}(z | x) := p(z | v, s), \quad v = \phi(x), \quad (18)$$

which depends on  $x$  only through  $v = \phi(x)$  (and, in the joint construction,  $s$ ).

Starting from (15), it suffices to prove that the induced joint over  $(Z, Y, S)$  is unchanged:

$$p_{\tilde{p}}(z, y, s) = p(z, y, s) \quad \forall z, y, s \implies I_{\tilde{p}}(Z; Y | S) = I_p(Z; Y | S). \quad (19)$$

Under  $p(z | x)$ , using semantic sufficiency  $p(y | x, s) = p(y | v, s)$  with  $v = \phi(x)$ ,

$$\begin{aligned} p(z, y, s) &= \sum_x p(z | x) p(y | x, s) p(x, s) = \sum_v p(y | v, s) p(v, s) \sum_{x:\phi(x)=v} \alpha_{x|v,s} p(z | x) \\ &= \sum_v p(y | v, s) p(v, s) p(z | v, s). \end{aligned} \quad (20)$$

Under  $\tilde{p}(z | x) = p(z | v, s)$ ,

$$\begin{aligned} p_{\tilde{p}}(z, y, s) &= \sum_x \tilde{p}(z | x) p(y | x, s) p(x, s) = \sum_v p(z | v, s) p(y | v, s) \sum_{x:\phi(x)=v} p(x, s) \\ &= \sum_v p(z | v, s) p(y | v, s) p(v, s) = p(z, y, s), \end{aligned} \quad (21)$$

so  $I_{\tilde{p}}(Z; Y | S) = I_p(Z; Y | S)$ .

Next, recall (16). For  $p$ , define  $p(z) := \sum_x p(z | x) p(x)$ . Grouping by  $(v, s)$  yields

$$I_p(Z; X) = \sum_{v,s} p(v, s) \sum_{x:\phi(x)=v} \alpha_{x|v,s} \sum_z p(z | x) \log \frac{p(z | x)}{p(z)}. \quad (22)$$

For  $\tilde{p}$ , the  $Z$ -marginal matches:

$$p_{\tilde{p}}(z) = \sum_x \tilde{p}(z | x) p(x) = \sum_{v,s} p(v, s) p(z | v, s) = \sum_{v,s} p(v, s) \sum_{x:\phi(x)=v} \alpha_{x|v,s} p(z | x) = p(z), \quad (23)$$

hence the denominator is unchanged. Therefore

$$I_{\tilde{p}}(Z; X) = \sum_{v,s} p(v, s) \sum_z p(z | v, s) \log \frac{p(z | v, s)}{p(z)}. \quad (24)$$

Define  $f(r) := \sum_z r(z) \log \frac{r(z)}{p(z)} = D_{\text{KL}}(r \| p(z))$ . By convexity of  $D_{\text{KL}}(\cdot \| p(z))$  in its first argument, for each fixed  $(v, s)$ ,

$$\begin{aligned} \sum_z p(z | v, s) \log \frac{p(z | v, s)}{p(z)} &= f\left(\sum_{x:\phi(x)=v} \alpha_{x|v,s} p(\cdot | x)\right) \leq \sum_{x:\phi(x)=v} \alpha_{x|v,s} f(p(\cdot | x)) \\ &= \sum_{x:\phi(x)=v} \alpha_{x|v,s} \sum_z p(z | x) \log \frac{p(z | x)}{p(z)}. \end{aligned} \quad (25)$$

Multiplying (25) by  $p(v, s)$  and summing over  $(v, s)$  yields

$$\begin{aligned} I_{\tilde{p}}(Z; X) &= \sum_{v,s} p(v, s) \sum_z p(z | v, s) \log \frac{p(z | v, s)}{p(z)} \leq \sum_{v,s} p(v, s) \sum_{x:\phi(x)=v} \alpha_{x|v,s} \sum_z p(z | x) \log \frac{p(z | x)}{p(z)} \\ &= \sum_{v,s} \sum_{x:\phi(x)=v} p(x, s) \sum_z p(z | x) \log \frac{p(z | x)}{p(z)} = \sum_x p(x) \sum_z p(z | x) \log \frac{p(z | x)}{p(z)} = I_p(Z; X), \end{aligned} \quad (26)$$

Follow the information-theoretic generalization framework of Xu and Raginsky [2017]. By Assumption A.2, Theorem 1 of Xu and Raginsky [2017] gives

$$|\mathbb{E}[L_{\text{POP}}(Z) - L_{\text{EMP}}(Z)]| \leq \sqrt{\frac{2\sigma^2}{n} I(Z; S)}. \quad (27)$$

By Assumption A.3,

$$I(Z; S) = \sum_{i=1}^n I(Z_i; X_i) = n I(Z; X). \quad (28)$$

Combining (27)–(28) yields

$$\text{GEN}(Z) := \mathbb{E}[|L_{\text{POP}}(Z) - L_{\text{EMP}}(Z)|] \leq \sqrt{\frac{2\sigma^2}{n}} I_p(Z; X). \quad (29)$$

Applying the same argument to  $\tilde{Z}$  gives

$$\text{GEN}(\tilde{Z}) \leq \sqrt{\frac{2\sigma^2}{n}} I_{\tilde{p}}(Z; X). \quad (30)$$

Finally, since  $I_{\tilde{p}}(Z; X) \leq I_p(Z; X)$ , we obtain

$$\text{GEN}(\tilde{Z}) \leq \text{GEN}(Z).$$

□

**Assumption A.4.** Fix  $t$  and let  $\hat{Y}_t = F(E_{\text{time},t}, \tilde{h}_1, \dots, \tilde{h}_K)$  with  $\tilde{h}_k = g_{t,k} h_k$  and  $g_{t,k} \in [0, 1]$ . Assume  $F$  is coordinate-wise  $L_k$ -Lipschitz in  $\tilde{h}_k$  (w.r.t.  $\|\cdot\|$ ):

$$|F(\dots, a, \dots) - F(\dots, b, \dots)| \leq L_k \|a - b\|, \quad \forall a, b \in \mathbb{R}^d, \forall k \in [K].$$

**Theorem A.5.** Under Assump. A.4, define  $\Delta_k := \|h_k^{\text{err}} - h_k^{\text{true}}\|$  and  $\tilde{h}_k^{\text{true}} := g_{t,k} h_k^{\text{true}}$ ,  $\tilde{h}_k^{\text{err}} := g_{t,k} h_k^{\text{err}}$ . Let  $E := E_{\text{time},t}$  and  $\hat{Y}_t^{\text{true}} := F(E, \tilde{h}_1^{\text{true}}, \dots, \tilde{h}_K^{\text{true}})$ ,  $\hat{Y}_t^{\text{err}} := F(E, \tilde{h}_1^{\text{err}}, \dots, \tilde{h}_K^{\text{err}})$ . Then

$$(\hat{Y}_t^{\text{err}} - \hat{Y}_t^{\text{true}})^2 \leq K \sum_{k=1}^K L_k^2 g_{t,k}^2 \Delta_k^2.$$

*Proof.* For  $k = 0, \dots, K$ , set  $\mathbf{z}^{(k)} := (g_{t,1} h_1^{\text{err}}, \dots, g_{t,k} h_k^{\text{err}}, g_{t,k+1} h_{k+1}^{\text{true}}, \dots, g_{t,K} h_K^{\text{true}})$ , so  $\mathbf{z}^{(0)} = (\tilde{h}_1^{\text{true}}, \dots, \tilde{h}_K^{\text{true}})$  and  $\mathbf{z}^{(K)} = (\tilde{h}_1^{\text{err}}, \dots, \tilde{h}_K^{\text{err}})$ . By telescoping and Assump. A.4,

$$|\hat{Y}_t^{\text{err}} - \hat{Y}_t^{\text{true}}| \leq \sum_{k=1}^K |F(E, \mathbf{z}^{(k)}) - F(E, \mathbf{z}^{(k-1)})| \leq \sum_{k=1}^K L_k \|g_{t,k} (h_k^{\text{err}} - h_k^{\text{true}})\| = \sum_{k=1}^K L_k g_{t,k} \Delta_k.$$

Apply  $(\sum_{k=1}^K a_k)^2 \leq K \sum_{k=1}^K a_k^2$  with  $a_k = L_k g_{t,k} \Delta_k$ . □

**Theorem A.6.** Let  $V = \phi(X) \in \mathcal{V}$  be the TESS primitives, where  $\mathcal{V} = \mathcal{V}_1 \times \dots \times \mathcal{V}_K$ ,  $|\mathcal{V}_k| = M_k$ , and  $|\mathcal{V}| =: M = \prod_{k=1}^K M_k$ . For  $g : \mathcal{V} \rightarrow [-1, 1]$ , define  $\hat{Y} = g(V)$ , squared loss  $\ell(\hat{y}, y) = (\hat{y} - y)^2$ , and

$$R(g) := \mathbb{E} \ell(g(V), Y), \quad \hat{R}_n(g) := \frac{1}{n} \sum_{i=1}^n \ell(g(V_i), Y_i).$$

Then  $\exists$  a universal  $C > 0$  s.t.  $\forall \delta \in (0, 1)$ , w.p.  $\geq 1 - \delta$  over  $n$  i.i.d. samples,

$$\sup_{g: \mathcal{V} \rightarrow [-1, 1]} |R(g) - \hat{R}_n(g)| \leq C \left( \sqrt{\frac{M}{n}} + \sqrt{\frac{\log(1/\delta)}{n}} \right).$$

In particular,  $n \gtrsim M/\varepsilon^2 \Rightarrow \sup_g |R(g) - \hat{R}_n(g)| \leq \varepsilon$ .

*Proof.* Define  $\mathcal{G} := \{g : \mathcal{V} \rightarrow [-1, 1]\}$  and its empirical Rademacher complexity

$$\hat{\mathfrak{R}}_n(\mathcal{G}) = \mathbb{E}_\sigma \left[ \sup_{g \in \mathcal{G}} \frac{1}{n} \sum_{i=1}^n \sigma_i g(V_i) \right], \quad \sigma_i \stackrel{iid}{\sim} \{\pm 1\}.$$

Group samples by primitive value and let  $N_v := |\{i : V_i = v\}|$  so that  $\sum_{v \in \mathcal{V}} N_v = n$ . Then

$$\sup_{g \in \mathcal{G}} \sum_{i=1}^n \sigma_i g(V_i) = \sup_g \sum_{v \in \mathcal{V}} g(v) \sum_{i: V_i=v} \sigma_i = \sum_{v \in \mathcal{V}} \left| \sum_{i: V_i=v} \sigma_i \right|.$$

Taking expectation over  $\sigma$  and using  $\mathbb{E}_\sigma |\sum_{j=1}^m \sigma_j| \leq \sqrt{m}$  yields

$$\widehat{\mathfrak{R}}_n(\mathcal{G}) \leq \frac{1}{n} \sum_{v \in \mathcal{V}} \sqrt{N_v}.$$

By Cauchy–Schwarz,

$$\sum_{v \in \mathcal{V}} \sqrt{N_v} \leq \sqrt{\left(\sum_v 1\right)\left(\sum_v N_v\right)} = \sqrt{Mn},$$

hence  $\widehat{\mathfrak{R}}_n(\mathcal{G}) \leq \sqrt{M/n}$ .

Since  $\ell(\cdot, y)$  is 4-Lipschitz on  $[-1, 1]$ , the contraction inequality gives

$$\widehat{\mathfrak{R}}_n(\ell \circ \mathcal{G}) \leq 4\widehat{\mathfrak{R}}_n(\mathcal{G}) \leq 4\sqrt{\frac{M}{n}}.$$

Applying the standard Rademacher generalization bound (e.g. Bartlett & Mendelson, 2002), with probability at least  $1 - \delta$ ,

$$\sup_{g \in \mathcal{G}} (R(g) - \widehat{R}_n(g)) \leq 2\widehat{\mathfrak{R}}_n(\ell \circ \mathcal{G}) + c\sqrt{\frac{\log(1/\delta)}{n}} \leq C\left(\sqrt{\frac{M}{n}} + \sqrt{\frac{\log(1/\delta)}{n}}\right),$$

for universal constants  $c, C > 0$ . The same bound holds for the absolute deviation.  $\square$

*Remark A.7.* Theorem A.6 gives a complexity term  $\sqrt{M/n}$  with  $M = \prod_k M_k$ , compared to the token-level  $\sqrt{\log |\mathcal{A}_T|/n}$ ; in particular, for  $|\mathcal{A}_T| = 2^T$  this improves  $\sqrt{T/n}$  to  $\sqrt{(\prod_k M_k)/n}$  when  $\prod_k M_k \ll T$ .

## B Detailed dataset statistics

Table 3: The Electricity dataset represents the half-hourly electricity demand in a state. FNSPID provides daily stock price data integrated with time-aligned financial news. Environment dataset contains daily Air Quality Index (AQI) measurements and Bitcoin denotes the daily Bitcoin price.

Datasets	Electricity	Bitcoin	FNSPID	Environment
<b>Time Horizon</b>	2019.01-2021.12	2019.01-2021.06	Not specified	1982.01-2012.05
<b>Variates</b>	19	18	7	4
<b>Timesteps</b>	52,560	858	49140	11,095
<b>Granularity</b>	30 minutes	1 day	5 days	7 days
<b>Input length</b>	48	7	5	7
<b>Prediction length</b>	48	7	5	7

We conduct experiments on four real-world multimodal datasets from diverse domains, namely Bitcoin, FNSPID, Electricity, and Environment. Each dataset consists of a target time series accompanied by temporally aligned news text describing relevant external events and contextual information.

The news corpus corresponding to each time series is collected from multiple financial news archives and publicly accessible news repositories, including established sources such as the Reuters News Archive. In addition, we gather supplementary news articles from Google News through third-party aggregation tools, which aggregate and index articles from a wide range of media outlets.

All collected news articles are timestamped and systematically aligned with the corresponding time-series observations based on their publication time, ensuring temporal consistency between the textual and numerical modalities. This alignment enables the model to effectively leverage contemporaneous textual information for time-series forecasting.

## C Detailed baseline configurations

To ensure fair comparison, we conduct systematic hyperparameter search on the validation set for all baseline methods. For architectural parameters, we maintain consistency across models where applicable: embedding dimension is uniformly set to 512, dropout rate to 0.1, and activation function primarily uses GELU. Most encoder-decoder architectures employ 2 encoder layers and 1 decoder layer to balance model capacity and avoid overfitting on smaller datasets.

Learning rate is the primary hyperparameter subject to grid search. For traditional time-series models, we search over three standard values: 0.0005, 0.0001, and 0.00005. Models exhibiting stable performance in preliminary experiments (e.g., TimesNet) directly adopt 0.0005 to reduce computational cost. For multimodal models with more complex training dynamics, the search range extends to [0.005, 0.001, 0.0001, 0.0005]. Additional architecture-specific searches include: decoder layers for FEDformer (1 or 2 layers), attention heads for PatchTST (ranging from 2 to 8), and factor parameters for Pyraformer (1 or 3). Dataset-specific adjustments are made when necessary. For instance, Pyraformer’s window size is adjusted to [4, 4] for Bitcoin’s short sequences, and TimeLLM’s top\_k is reduced to 3 for smaller datasets like FNSPID.

## D Prompts

In this section, we list the prompt template we use throughout the paper. Other than ensuring that generations could be parsed properly, our prompt were not optimized towards any particular models.

### D.1 Template for Temporal Evolution Primitives Extraction

#### Prompt Template

```
You are a professional {role from the dataset background}.
Your task is to analyze the provided textual information and
infer temporal evolution patterns that may impact future time series behavior.
```

```
Textual Input: {text_content}
Domain Context: {domain_context}
```

```
Instructions:
```

```
Based on the textual content provided below, analyze and classify
the following four temporal evolution primitives:
```

1. Mean Shift - Infer the direction and magnitude of anticipated level changes:  
<strong-rise | mild-rise | stable | mild-drop | strong-drop>
2. Volatility - Infer the anticipated changes in volatility regime:  
<surge | rise | stable | fall | calm>
3. Shape - Infer the dominant trend morphology pattern over the forecast horizon:  
<ascend | descend | peak | trough | oscillate>
4. Lag and Decay - Infer the temporal localization and persistence of the impact:  
<early-fade | early-persist | mid-fade | mid-persist | late | diffuse>

```
You MUST output in the following EXACT format with no extra text:
```

```
Mean Shift: <strong-rise | mild-rise | stable | mild-drop | strong-drop>
Volatility: <surge | rise | stable | fall | calm>
Shape: <ascend | descend | peak | trough | oscillate>
```

Lag: <early-fade | early-persist | mid-fade | mid-persist | late | diffuse>

Provide your analysis in the exact format specified above.